The Scales and Equilibration of Midocean Eddies: Freely Evolving Flow

K. SHAFER SMITH AND GEOFFREY K. VALLIS

Geophysical Fluid Dynamics Laboratory, Princeton University, Princeton, New Jersey

(Manuscript received 8 December 1999, in final form 8 May 2000)

ABSTRACT

Quasigeostrophic turbulence theory and numerical simulation are used to study the mechanisms determining the scale, structure, and equilibration of mesoscale ocean eddies. The present work concentrates on using freely decaying geostrophic turbulence to understand and explain the vertical and horizontal flow of energy through a stratified, horizontally homogeneous geostrophic fluid. It is found that the stratification profile, in particular the presence of a pycnocline, has significant, qualitative effects on the efficiency and spectral pathways of energy flow. Specifically, with uniform stratification, energy in high baroclinic modes transfers directly, quickly (within a few eddy turnaround times), and almost completely to the barotropic mode. By contrast, in the presence of oceanlike stratification, kinetic energy in high baroclinic modes transfers intermediately to the first baroclinic mode, whence it transfers inefficiently (and incompletely) to the barotropic mode. The efficiency of transfer to the barotropic mode is reduced as the pycnocline is made increasingly thin. The β effect, on the other hand, improves the efficiency of barotropization, but for oceanically realistic parameters this effect is relatively unimportant compared to the effects of nonuniform stratification. Finally, the nature of turbulent cascade dynamics is such as to lead to a concentration of first baroclinic mode kinetic energy near the first radius of deformation, which, in the case of a nonuniform and oceanically realistic stratification, has a significant projection at the surface. This may in part explain recent observations of surface eddy scales by TOPEX/Poseidon satellite altimetry, which indicate a correlation of surface-height variance with the scale of the first deformation radius.

1. Introduction

Over the last two decades or so it has become increasingly apparent that the ocean is literally a sea of eddies. In midlatitudes these eddies arise primarily from baroclinic instability of the mean flow, although in some regions barotropic instability may also be important. Although the linear theory of the processes that give rise to such eddies is well understood, the presumably nonlinear processes that determine how and at what scales these eddies ultimately equilibrate are less so. The latter is the subject of this paper.

Recent satellite altimeter measurements of the ocean surface by the TOPEX/Poseidon experiment (e.g., Stammer 1997) have renewed interest in this problem. Time series from satellite measurements such as these are not yet long enough to analyze interannual phenomena, but are rich in information relevant to short timescale eddy dynamics. A particularly puzzling result regards the horizontal length scale of the eddies, as manifested in the surface height field—surface eddy scales appear linearly correlated with the first baroclinic radius of deformation, L_{Ro}. This result is surprising for two reasons. First, while we know baroclinic instability to be the source of most mesoscale ocean eddies (e.g., Gill et al. 1974; Beckman et al. 1994), the scale of midocean baroclinic instability itself need not be at the deformation scale. If, for example, the thermocline contains two maxima in stratification, separated by mode water, as over much of the subtropical gyres (Samelson and Vallis 1997), then the fastest growing mode may have scales much smaller than the deformation scale, due to a *defect instability*, which results from kinks in the vertical profiles of shear or mean velocity (Samelson 1999). Thus, in general, the deformation scale does not correspond to the most unstable wavelength. [This is also true for the problem of Charney (1947)]. The second reason is that, in a turbulent geostrophic fluid, we should expect an inverse cascade of energy to scales much larger than the deformation scale, interrupted only by the β effect, friction, or the domain scale itself (e.g., Rhines 1975; Maltrud and Vallis 1991). One measure of the halting scale produced by the gradient of planetary vorticity (β) is the scale $L_\beta \simeq \sqrt{\upsilon_{\mathrm{rms}}/\beta}$, where υ_{rms} is the root-mean-square barotropic velocity (Rhines 1975). Stammer compares the horizontal scale of maximal eddy kinetic energy (EKE) with both L_{Ro} and L_β as a function of latitude—the result demonstrates a correlation of peak EKE scale with L_{Ro}, and not with L_β.

Corresponding author address: Dr. K. Shafer Smith, Geophysical Fluid Dynamics Laboratory, Princeton University, P.O. Box 308, Princeton, NJ 08542.
E-mail: kss@gfdl.gov

Our lack of understanding concerning the (measurable) surface scales of eddies raises other important questions. Mean current profiles are generated primarily by wind stress, concentrating the shear near the ocean surface. Thus, one also expects eddy generation from baroclinic instability to occur primarily near the surface. How, then, do eddies, which are at least initially surface intensified and far from any boundaries (where energy might be lost in the form of lateral or bottom drag), come to steady state with the mean flow? Classical geostrophic turbulence theory (e.g., Charney 1971) would argue that turbulence in a (uniformly) stratified geostrophic fluid leads to an inverse energy cascade in both vertical *and* horizontal scale, which would lead us to expect these initially surface intensified (hence baroclinic) eddies to barotropize, allowing bottom friction to ultimately limit their growth. But barotropic eddies must certainly be unconcerned with any (baroclinic) deformation scale, so that, if we believe the satellite data, the picture of eddy energy evolving quite efficiently into barotropic energy cannot be the whole story.

In sum, the mechanisms that set the scales and magnitudes of mesoscale ocean eddies, and bring them to statistical steady state with the mean flow, are not fully understood. This paper concentrates on understanding the dynamics of the energetic transfers in perhaps the simplest relevant setting: freely evolving quasigeostrophic flow (Pedlosky 1987) in an oceanically realistic, fixed, stratification. A second paper will consider the arguably more oceanically relevant, and certainly more complex, forced-dissipative dynamics. We motivate our approach and briefly review relevant existing theory in section 2. Section 3 lays the groundwork for the theory that is developed in 4. Numerical simulations are described in section 5, and the paper concludes in section 6.

2. Geostrophic turbulence in the ocean

Geostrophic turbulence in the ocean, and hence the processes of equilibration of baroclinic eddies, is to be distinguished between the corresponding processes in the atmosphere in (at least) two significant ways. First, the deformation scale in the troposphere is $O(1000$ km), so that its ratio to the domain size is not too much smaller than unity, while in the ocean the deformation scale is $O(50$ km), yielding a significant scale separation from the basin size. Second, in the troposphere the mean stratification is fairly uniform, whereas in the ocean there is a sharp gradient in potential density near the surface, that is, the thermocline. The buoyancy frequency, $N(z)$, is thus nearly an order of magnitude larger in the thermocline than in the abyss. Likewise, the mean velocity shear in the atmosphere is roughly uniform, while in the ocean it is concentrated, like the thermocline, within the uppermost kilometer.

The oceanic case has some aspects that are simpler and some more challenging to understand. The lack of a significant scale separation between eddy and mean flow in the atmosphere leads to the possibility of order–unity feedback by the eddies onto the mean flow that generated them. In this way they may in fact aid in their own equilibration by stabilizing the mean circulation, as in the baroclinic adjustment hypothesis (Stone 1978), although other equilibration mechanisms undoubtedly also occur (e.g., Vallis 1988). Although there exists an oceanic analog, namely the homogenization of potential vorticity in gyres (Rhines and Young 1982), the mean shear and stratification are to lowest-order consequences of the very-large scale, quasi-steady, wind and buoyancy driven circulation, and it seems unlikely that oceanic eddies can equilibrate *solely* by modifying these properties to bring about a stable mean state. While this hypothesis needs to be tested explicitly, we feel its reasonable, in the first instance, to consider eddy-induced alterations to the mean state as perturbative in scale.

In the ocean, then, in some contrast to the atmosphere, it may be sensible to separate the effect of the mean flow and stratification on the eddies from the effect of the latter on the former. The same attribute of oceanic variability that makes this a sensible first approximation, namely the large-scale separation between the baroclinic radii of deformation and the scale of the mean circulation, allows for the possibility of a significant cascade of energy between scales. These features together imply that significant understanding of ocean eddy dynamics may be gained through the modeling of geostrophic turbulence on a fixed stratification and mean flow background. Furthermore, quasigeostrophic scaling will usually hold for oceanic domains chosen to be on $O(10L_{\mathrm{Ro}})$. Thus the use of the stratified quasigeostrophic equations in a model with periodic boundaries is well posed for the study of eddies in localized regions of the ocean. Allowing us to *specify* the stratification and mean shear simplifies the problem in one sense, although it means that we must seek a nonlinear mechanism of equilibration a priori.

The second characteristic difference, the nonuniformity of stratification and mean shear, is an unambiguously complicating factor. The surface intensified nature of the mean stratification and shear leads us to expect that eddy generation occurs near the surface, and poses the possibility that the eddies *remain* surface intensified. By contrast, typical models of geostrophic turbulence (with uniform stratification) give rise to baroclinic instability more uniformly throughout the interior and need only a linear bottom drag (mimicking the effect of Ekman layer) to remove energy from the system. It is by no means clear that this will be sufficient in the more oceanic case, and we are still left with the question: *How can eddy energy, generated near the surface, be dissipated, and hence bring the system to a statistical steady state?* The sufficiency of bottom drag would imply efficient downward transfer of energy, likely as barotropization of the eddies. This may of course be a red herring, as it is possible that other effects not included

in such a limited model (e.g., topography) may further inhibit this transfer. But certainly, the possible *insufficiency* of bottom drag in bringing the system to equilibrium would imply the existence of alternate energy removal or transfer mechanisms in the ocean, where in fact a statistical steady state exists.

The current work is intended to be a step toward modeling turbulent behavior in a more realistic (though still quite idealized) oceanic setting, thereby gaining a more complete understanding of the interplay between turbulent eddy dynamics and the large-scale dynamics of the ocean. This task necessitates a small extension of geostrophic turbulence theory, particularly as it applies to regimes with nonuniform stratification.

3. Quasigeostrophic preliminaries

Equations of motion

The evolution equation for the unforced, nearly inviscid, quasigeostrophic perturbation potential vorticity, $q = q(x, y, z, t)$, is

$$q_t + J(\psi, q) + \beta\psi_x = -\nu\nabla^8 q, \tag{3.1}$$

where ν is a hyperviscosity parameter, $J(a, b) = a_x b_y - a_y b_x$ is the Jacobian operator, and β is the meridional gradient of the Coriolis parameter, f. Hyperviscosity is used as a scale-selective dissipation mechanism, essentially as a subgrid-scale parameterization, to absorb small-scale enstrophy. The perturbation potential vorticity is related to the perturbation streamfunction, $\psi(x, y, z, t)$, by

$$q = \nabla^2\psi + \frac{d}{dz}\left[S(z)^2\frac{d\psi}{dz}\right], \tag{3.2}$$

where $\nabla^2\psi = \psi_{xx} + \psi_{yy}$ and $S(z) = f/N(z)$ is the ratio of the Coriolis frequency, f, to the buoyancy frequency, $N(z)$.

We can project ψ onto a Fourier series in the x, y plane,

$$\psi(x, y, z, t) = \sum_{k,l} \psi_{kl}(z, t)e^{i(kx+ly)}, \tag{3.3}$$

in which case spectral components will be distinguished from their physical counterparts by the presence of the wave-vector subscripts, k, l. The reality of the physical field implies that $\psi_{kl} = \psi^*_{-k,-l}$. Substitution of (3.3) into (3.1) yields the spectral equations of motion

$$\dot{q}_{kl} + \hat{J}_{kl}(\psi, q) + ik\beta\psi_{kl} = -\nu K^8 q_{kl}, \tag{3.4}$$

where

$$q_{kl} = \left[-K^2 + \frac{d}{dz}S(z)^2\frac{d}{dz}\right]\psi_{kl}, \tag{3.5}$$

and the Jacobian term is understood now to represent the full spectral sum of the nonlinear products of the spectral coefficients, and $K^2 = k^2 + l^2$. Numerical integration of these equations is most efficiently performed in height coordinates (see appendix), but to understand energetic transfers a transformation to vertical modes is convenient.

NORMAL MODES

The vertical normal modes, or stratification modes ϕ, and the baroclinic deformation wavenumbers, λ, are the eigenvalues and eigenfunctions of the vertical differencing operator in (3.2), which is the Sturm–Liouville equation

$$\frac{d}{dz}\left(S(z)^2\frac{d\phi}{dz}\right) = -\lambda^2\phi, \qquad z \in (-H, 0), \tag{3.6}$$

with the boundary conditions $d\phi/dz = 0$ at $z = 0, -H = 0$ (i.e., a rigid lid and flat bottom). We demand that the modes be orthonormal, which yields the condition,

$$\int_{-H}^{0} \phi_i\phi_j\, dz = \delta_{ij}, \tag{3.7}$$

where δ_{mn} is the Kronecker delta, and the subscripts refer to the mode numbers ($m = 0$ for the barotropic mode, $m = 1$ for the first baroclinic mode, etc.).

The quasigeostrophic equation of motion can be projected onto these modes (following, e.g., Flierl 1978; Hua and Haidvogel 1986) utilizing the orthonormality of the eigenfunctions, ϕ_m. We will consistently represent the modal components by uppercase symbols. We expand the streamfunction

$$\psi_{kl}(z, t) = \sum_{m=0}^{\infty} \Psi_{klm}(t)\phi_m(z), \tag{3.8}$$

which upon substitution into (3.4) and integration over z yields the equation of motion for the spectral triplet (klm)

$$\dot{Q}_{klm} + \sum_{i,j} \varepsilon_{mij}\hat{J}_{kl}(\Psi_i, Q_j) + ik\beta\Psi_{klm} = -\nu K^8\Psi_{klm}, \tag{3.9}$$

where

$$Q_{klm} = -(k^2 + l^2 + \lambda_m^2)\Psi_{klm} \tag{3.10}$$

and $\hat{J}_{kl}(\,,\,)$ is shorthand for the spectral Jacobian.

The triple interaction coefficient, ε_{mij} arises as the factor controlling the strength of nonlinear mode coupling and in the modal forcing. This coefficient is given by the vertical integral over the product of the vertical modes in the triplet,

$$\varepsilon_{mij} = \int_{-H}^{0} \phi_m\phi_i\phi_j\, dz. \tag{3.11}$$

In the case where all mode numbers are the same, the coefficient gives the strength of the self-interaction of that mode, or in a loose sense, the resistance of energy in that mode to transfer to another mode. Note also that its presence in the summation over the nonlinear Ja-

cobian terms in (3.9) makes the direct use of the modal equation in numerical code highly inefficient—each time step then requires multiple executions of the most time-consuming calculation. This inefficiency is made extreme when the stratification is nonuniform—in this case, there are very few zeros in the coefficient ε_{mij} and the calculation becomes huge, growing roughly as the cube of vertical resolution.

Modal energy budgets are formed via multiplication of (3.9) by $-\Psi^*_{klm}$, whence

$$\dot{E}_{klm} = T_{klm} + H_{klm}, \tag{3.12}$$

where the individual terms on the right-hand side represent the energetic rates into mode (klm) of, respectively, internal transfers and the hyperviscous dissipation. Note that the sum over wavenumbers and modes of T_{klm} is formally zero, and that, due to the presumed inverse cascade, H_{klm}, when summed, is small. Expressions for the kinetic and available potential energy spectra, whose sum is E_{klm}, are, respectively,

$$\mathcal{K}_{klm} = K^2|\Psi_{klm}|^2, \tag{3.13}$$

$$\mathcal{A}_{klm} = \lambda_m^2|\Psi_{klm}|^2. \tag{3.14}$$

Budget and energy spectra will be used later to diagnose numerical results. In this usage, they will generally be summed in shell-integral form over isotropic horizontal wavenumber, $K = \sqrt{k^2 + l^2}$.

4. Effects of nonuniform stratification: Theory

Here we seek to apply geostrophic turbulence theory to the case in which the mean stratification is nonuniform, and in particular to the case in which the stratification is concentrated in an upper region whose depth is a small fraction of the total. The goal is a general picture of the eddy production and internal energy transfer dynamics. We concentrate specifically on how the shape of the thermocline affects key scales, such as the first radius of deformation, and on the strength of energetic transfers between modes.

The simplest system that can represent nonuniform stratification is the two-layer quasigeostrophic model with unequal layer thicknesses. We thus investigate this first, followed by a more general treatment of the fully stratified case.

a. Two-layer case

We begin by investigating the normal modes of a system with two layers of generally unequal thickness. In the discretized system considered here the eigenvalue equation (3.6) becomes the two-by-two system of linear equations

$$\frac{1}{\delta_n}(\phi_{3-n} - \phi_n) = -\overline{\lambda}^2\phi_n, \qquad n = 1, 2, \tag{4.1}$$

where $\overline{\lambda}^2 \equiv \lambda^2(Hg\Delta\rho/f_0^2)$, in which $\Delta\rho$ is the density difference between layers, δ_n is the fractional thickness of the nth layer and λ is the original eigenvalue in (3.6) (or, the separation constant that arises when separation of variables is applied to the stratified quasigeostrophic equation). Nondimensional variables are denoted by an overbar. This system has eigenvalues

$$\overline{\lambda}_0 = 0, \qquad \overline{\lambda}_1 = \left(\frac{1}{\delta_1} + \frac{1}{\delta_2}\right)^{1/2}.$$

The second eigenvalue ($\overline{\lambda}_1$) is that of the baroclinic, or internal mode; since this is what we are concerned with, we drop its subscript. For clarity, we define $\delta \equiv \delta_1$ and write the lower layer thickness as $\delta_2 = 1 - \delta$. In this case the baroclinic eigenvalue is

$$\overline{\lambda} = \frac{1}{\sqrt{\delta(1 - \delta)}}. \tag{4.2}$$

If we consider the two-layer system most relevant to the ocean, then $\delta \ll 1$, so that $\overline{\lambda} \sim \delta^{-1/2}$.

The normalized eigenvector corresponding to this eigenvalue is

$$\boldsymbol{\phi}_{bc} = \begin{pmatrix} \sqrt{(1 - \delta)/\delta} \\ -\sqrt{\delta/(1 - \delta)} \end{pmatrix}.$$

Note that in this two-layer case the vertical integral in (3.7), used in normalization, is replaced by the vector product weighted by the fractional layer thicknesses (δ_n) as

$$\int_{-H}^{0} dz \to \sum_{n=1}^{N} \delta_n.$$

We can now calculate the interaction coefficients from (3.11). There are in fact only three possible values. In any case where one of the modes is the barotropic mode (say $l = 0$), the resulting integral is that of the product of two modes, which by the orthonormality condition yields

$$\varepsilon_{0ij} = \delta_{ij}, \tag{4.3}$$

and all permutations thereof, hence this accounts for two of the three possibilities. The exceptional case is the interesting case—namely the baroclinic self-interaction term, whose value is

$$\varepsilon_{111} = \frac{1 - 2\delta}{\sqrt{\delta(1 - \delta)}}. \tag{4.4}$$

Plainly, in the case of equal layer thickness ($\delta = ½$), the interaction vanishes. In the oceanlike case $\delta \ll 1$, implying $\varepsilon_{111} \sim \delta^{-1/2}$, just as for the deformation wavenumber.

To illustrate explicitly the relevance of this factor in the equations of motion, we write the two-layer form of (3.9) in physical space,

$$\frac{\partial}{\partial t}(\nabla^2\psi) + J(\psi, \nabla^2\psi) + J(\tau, \nabla^2\tau) + \beta\frac{\partial}{\partial x}\psi = 0, \tag{4.5}$$

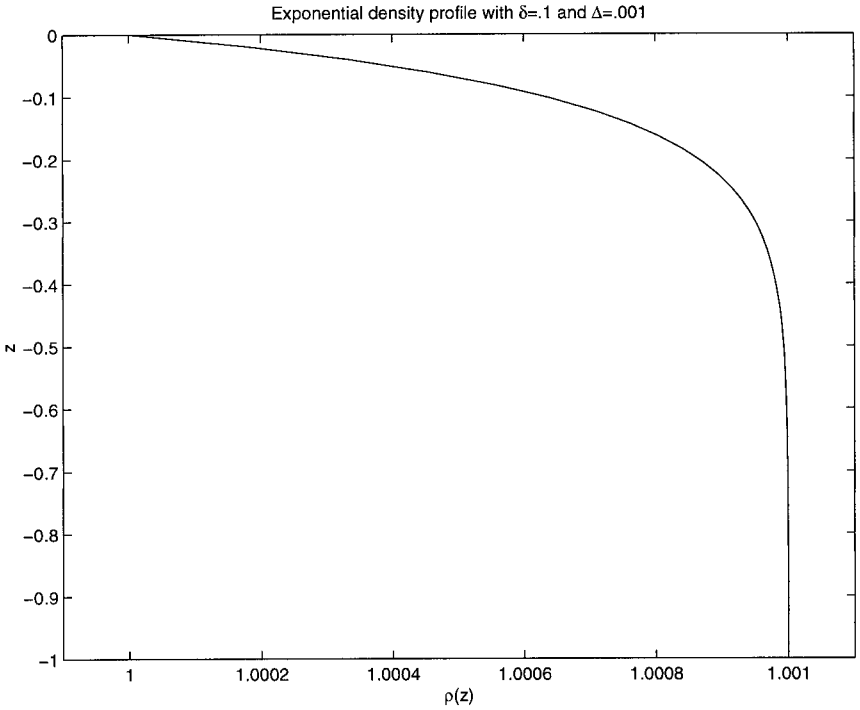

FIG. 1. Exponential density profile with $\delta = 0.1$ and $\Delta = 0.001$.

$$\frac{\partial}{\partial t}(\nabla^2\tau - \lambda^2\tau) + J(\psi, \nabla^2\tau - \lambda^2\tau) + J(\tau, \nabla^2\psi) + \varepsilon J(\tau, \nabla^2\tau) + \beta\frac{\partial}{\partial x}\tau = 0, \quad (4.6)$$

where $\psi \equiv \Psi_0$, $\tau \equiv \Psi_1$, $\varepsilon \equiv \varepsilon_{111}$ and λ is as in (4.2). Only one term, the baroclinic self-advection term in the baroclinic evolution equation (4.6), is affected by ε—its strength is thus modulated by the thickness of the thermocline and vanishes in the special case of uniform stratification.

b. *Continuously stratified case*

To proceed, we choose a density profile. A suitable nondimensional form is

$$\overline{\rho}(\overline{z}) = 1 + \Delta(1 - e^{\overline{z}/\delta}), \quad (4.7)$$

where $\Delta\rho \equiv (\rho_{\text{bottom}} - \rho_{\text{top}})/\rho_0$ is the fractional change in density over the depth of the ocean, $\delta \equiv a/H$ is the fractional scale depth, and $\overline{z}$ is the fractional depth coordinate, defined as $\overline{z} \equiv z/H$ (see Fig. 1).

The buoyancy frequency is $N^2(z) = -(g/\rho r_0)dp/dz$, which we nondimensionalize, $\overline{N}^2(\overline{z}) = (H/g')N^2(z)$, where $g' \equiv g\Delta\rho$. In terms of our density profile, this is

$$\overline{N}^2(\overline{z}) = \frac{e^{\overline{z}/\delta}}{\delta}. \quad (4.8)$$

With these definitions we have the nondimensional, explicit form of the mode equation (3.6),

$$\frac{d}{d\overline{z}}\left(\frac{1}{\overline{N}^2(\overline{z})}\frac{d\phi}{d\overline{z}}\right) = -\overline{\lambda}^2\phi, \qquad \overline{z} \in (-1, 0), \quad (4.9)$$

in which $\overline{\lambda}^2 \equiv (g'H/f_0^2)\lambda^2$.

To solve (4.9), we apply the WKB approximation of Chelton et al. (1998), who consider the related vertical velocity eigenvalue equation,

$$\frac{d^2w}{d\overline{z}^2} + \overline{N}^2\overline{\lambda}^2 w = 0, \qquad w(z = 0, -1) = 0, \quad (4.10)$$

to which they derive general approximate solutions

$$w_m(\overline{z}) \simeq B\sqrt{\frac{1}{\overline{\lambda}_m\overline{N}(\overline{z})}}\sin\left(\overline{\lambda}_m\int_{-1}^{\overline{z}}\overline{N}(\overline{z}')\,d\overline{z}'\right), \quad (4.11)$$

where the eigenvalues are

$$\overline{\lambda}_m \simeq \left(\frac{1}{m\pi}\int_{-1}^{0}\overline{N}(\overline{z}')\,d\overline{z}'\right)^{-1}, \qquad m \in [1, 2, \cdots, \infty). \quad (4.12)$$

Substitution of (4.8) into (4.12) yields

$$\overline{\lambda}_m \simeq \frac{m\pi}{2\sqrt{\delta}}, \quad (4.13)$$

and we see again that the deformation wavenumbers scale as $\delta^{-1/2}$, just as for the two-layer case.

The streamfunction modes of (4.9) are related to the vertical velocity modes by

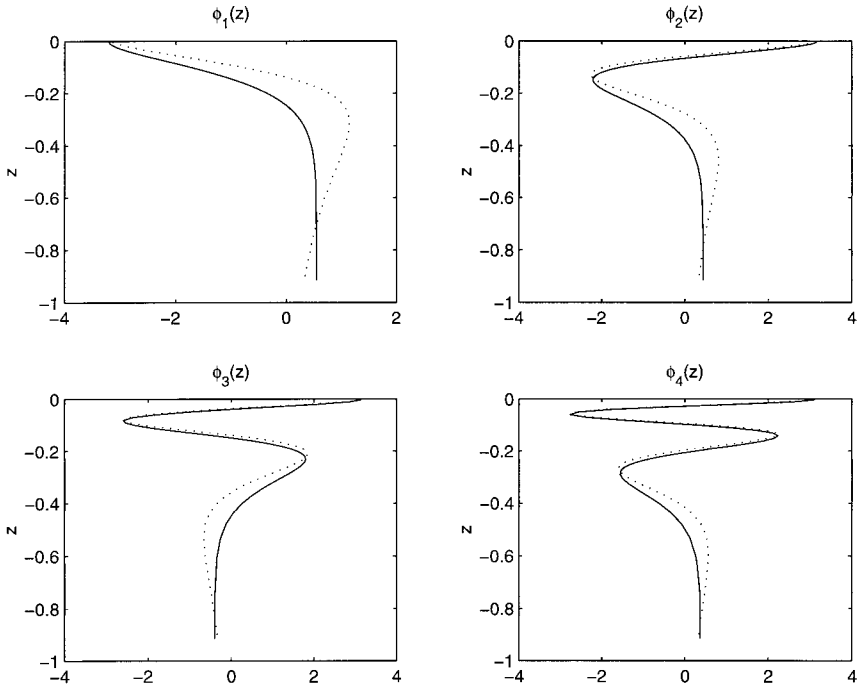

FIG. 2. Comparison of WKB approximation to numerical solution of first four baroclinic vertical modes, with $\delta = 1/10$. Solid lines are the numerical solutions and broken lines are the analytical approximation.

$$\phi_m(\overline{z}) = \overline{\lambda}_m \int_{-1}^{\overline{z}} \overline{N}^2(\overline{z}')w_m(\overline{z}')\, d\overline{z}', \qquad (4.14)$$

whence with the explicit form of $\overline{N}(\overline{z})$ in (4.8) we have

$$\phi_m(\overline{z}) \simeq \frac{B}{\delta}\sqrt{\frac{m\pi}{2}} \int_{-1}^{\overline{z}} e^{3\overline{z}'/4\delta} \sin(m\pi e^{\overline{z}'/2\delta})\, d\overline{z}'. \qquad (4.15)$$

In order to calculate explicit triple interaction coefficients we must derive a closed form for the eigenfunctions (4.15). The integral therein (whose value we will refer to as I) can be rewritten in terms of the substitution $x = e^{\overline{z}'/2\delta}$,

$$I = \frac{1}{\delta}\int_{-1}^{\overline{z}} e^{3\overline{z}'/4\delta} \sin(m\pi e^{\overline{z}'/2\delta})\, d\overline{z}'$$

$$= \int_0^{e^{\overline{z}/2\delta}} x^{1/2} \sin(m\pi x)\, dx, \qquad (4.16)$$

where the lower limit of integration is approximated as 0 under the assumption $\delta \ll 1$. The result of the *indefinite* integral is

$$I(x) = -\frac{1}{m\pi}\left[\sqrt{x}\cos(m\pi x) + \frac{1}{\sqrt{2m}}C(\sqrt{2mx})\right],$$

where $C(x)$ is the Fresnel cosine function (Abromowitz and Stegun 1972, section 7.3). Evaluated at the lower limit, $I(0) = 0$. The upper limit, $x = e^{\overline{z}/2\delta}$, is always less than 1 for the domain of integration, so it may be advantageous to consider an expansion of $C(x)$. In fact,

$$C(x) = \frac{x}{3}\cos\left(\frac{\pi}{2}x^2\right) + O(x^5),$$

so that for all values of x_u in our domain, the higher-order terms are truly negligible, and hence

$$I(x_u) \simeq -\frac{2\sqrt{x_u}}{3m\pi}\cos(m\pi x_u).$$

Substituting this result into (4.15) (and absorbing numerical constants into a redefined constant B), we have

$$\phi_m(\overline{z}) \simeq B\sqrt{\frac{2}{m\pi}}e^{\overline{z}/2\delta}\cos(m\pi e^{\overline{z}/2\delta}), \qquad m \geq 1,$$

which form an orthogonal set of basis functions. The additional requirement that $m \geq 1$ is all right since for the barotropic mode ($\lambda_0 = 0$), $\phi_0 = 1$ is obviously a solution to (4.9). Requiring orthonormality via (3.7), we find that $B = \sqrt{m\pi/2\delta}$ so that the normalized eigenfunctions are

$$\phi_m(\overline{z}) \cong \delta^{-1/2}e^{\overline{z}/2\delta}\cos(m\pi e^{\overline{z}/2\delta}), \qquad m \geq 1. \quad (4.17)$$

In Fig. 2 we compare numerical solutions of (4.9) to this analytical approximation for the first four baroclinic modes in a case with $\delta = 0.1$. Given that our goals in this study are but *semi*-quantitative, the agreement of the fit with the ''true'' curves is perfectly sufficient.

Finally, using (4.15) in (3.11) we can explicitly calculate triple interaction coefficients,

$$\varepsilon_{lmn} \simeq \delta^{-3/2} \int_{-1}^{0} e^{3\bar{z}/4\delta} \cos(l\pi e^{\bar{z}/2\delta}) \cos(m\pi e^{\bar{z}/2\delta}) \cos(n\pi e^{\bar{z}/2\delta})\, d\bar{z}, \tag{4.18}$$

which can be solved using the same substitution ($x = e^{\bar{z}/2\delta}$) used to get (4.16). The resulting integral is

$$\varepsilon_{lmn} \simeq 2\delta^{-1/2} \int_{0}^{1} x^{1/2} \cos(l\pi x) \cos(m\pi x) \cos(n\pi x)\, d\bar{z}. \tag{4.19}$$

This is solvable again in terms of Fresnel functions, but a few comments are in order regarding the result so far. First, the integral is now a purely numerical function of the mode numbers, and in fact the result will obviously be independent of their permutations (as it should be). Second, all of the factors in the integrand are bounded on [0, 1], so that the integral itself, which has the same range, is order unity. Third, if one of the modes is the barotropic mode, then the same argument applies as for the two-layer case and again (4.3) holds. Hence we arrive at the interesting fact that *all of the coefficients except those with transfers into the barotropic mode scale as* $\delta^{-1/2}$. This means that internal transfers between baroclinic modes can occur with relatively greater efficiency than can transfers to (or from) the barotropic mode. We will return to this important point later.

Eigenvalues (deformation wavenumbers) and triple interaction coefficients are calculated numerically for the range of thermocline thickness $\delta \in [0.05, 0.3]$ and the results are plotted in Fig. 3 against $\delta^{-1/2}$. Both curves are essentially linear, verifying the scaling result. Note that the slight variation from linearity in the curve for λ_1 occurs where δ is becoming large, hence the approximations made based on its smallness start to break down.

For the sake of completeness we give the explicit result,

$$\begin{aligned}\varepsilon_{lmn} \simeq \frac{1}{2\pi\sqrt{\delta}}\Bigg[&\frac{\sin(\pi f_{l,m,n})}{f_{l,m,n}} + \frac{\sin(\pi f_{l,m,-n})}{f_{l,m,-n}} + \frac{\sin(\pi f_{l,-m,n})}{f_{l,-m,n}} \\ &+ \frac{\sin(\pi f_{l,-m,-n})}{f_{l,-m,-n}} - \frac{S(\sqrt{2 f_{l,m,n}})}{\sqrt{2}\, f_{l,m,n}^{3/2}} \\ &- \frac{S(\sqrt{2 f_{l,m,-n}})}{\sqrt{2}\, f_{l,m,-n}^{3/2}} - \frac{S(\sqrt{2 f_{l,-m,n}})}{\sqrt{2}\, f_{l,-m,n}^{3/2}} \\ &- \frac{S(\sqrt{2 f_{l,-m,-n}})}{\sqrt{2}\, f_{l,-m,-n}^{3/2}}\Bigg],\end{aligned}$$

where $f_{lmn} = l + m + n$ and $S(x)$ is the Fresnel Sine series (see again Abromowitz and Stegun 1972). The Fresnel functions start from 0 and oscillate about ½ as their argument increases. Hence for all modal triplets, the numerical factor is $O(1)$ and hence the interaction coefficient is $O(\delta^{-1/2})$. As a useful example, the first baroclinic self-interaction term is $\varepsilon_{111} \cong (0.255)\delta^{-1/2}$.

c. Energetic transfers

In the case of two layers of equal thickness, large-scale baroclinic energy evolves essentially as a passive tracer being advected by the barotropic flow, and is thus likely to cascade directly toward smaller scales (Salmon 1980; also Rhines 1977). On the other hand, at small scales vortex stretching is very weak and layers are essentially decoupled—in this case small-scale energy will cascade inversely toward larger scales in each layer separately. The separation scale between these two regimes is the radius of deformation. Ultimately, then, energy in baroclinic modes will cascade from either direction toward the first baroclinic radius of deformation. It will then proceed to cascade toward the barotropic scales and, unless this process is somehow less efficient, there is no reason to expect a build up of energy at the deformation scale.

With two layers of unequal thickness, or in the continuously stratified cases with a pycnocline, transfers involving the barotropic mode are independent of δ, while all others scale as $\delta^{-1/2}$. Hence as the thermocline becomes thinner, the relative strength of the baroclinic advection of baroclinic energy *increases* over the strength of both transfers into the barotropic mode and over barotropic self-advection. Thus, if *all* of the internal baroclinic energy transfers are enhanced, *and* presuming that turbulent geostrophic energy does indeed move toward large *isotropic* scale, then we should expect energy in high modes to concentrate in the first baroclinic mode, since energy there is relatively inhibited from transfer into the barotropic mode.

Our argument that energy may concentrate in the first baroclinic mode is consistent with that of Fu and Flierl (1980). They demonstrate, through calculations involving the relative growth rates of triad Rossby wave instabilities in continuously but oceanically stratified, quasigeostrophic motion, that energy in high baroclinic modes should preferentially transfer to the first baroclinic mode (in agreement with the argument of the previous paragraph), from whence it is expected to cascade from *either direction* toward the first radius of deformation. From here the energy can transfer to the barotropic mode, albeit with reduced efficiency over the uniformly stratified case. Once in the barotropic mode it is expected to cascade upscale toward an arrest scale (likely set by planetary β and/or frictional effects). This differs significantly from the uniformly stratified case, in which energy in high baroclinic modes may transfer

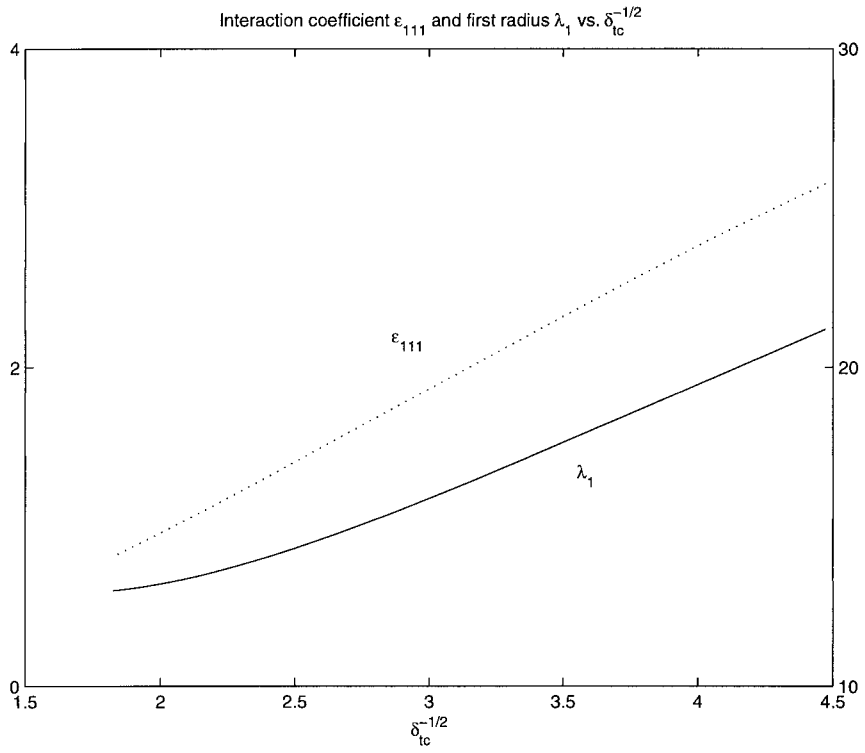

FIG. 3. Left axis corresponds to dashed line (ϵ_{111}) and solid line (λ_1) corresponds to right axis.

directly to the barotropic mode. A schematic of the transfer preferences is shown in Fig. 4. The preference of transfers from high modes to the first baroclinic mode can be understood intuitively, as pointed out by Fu and Flierl, as a result of the surface intensification of the vertical modes—it is more difficult for high mode energy concentrated near the surface to spread directly to motion, which is constant with depth. Furthermore, this concentration will be enhanced by any inhibition of transfers to the barotropic mode.

Finally, statistical mechanical arguments (Salmon et al. 1976) seem to suggest that, with a thin upper layer, a secondary peak near the deformation scale will be found in the upper-layer kinetic energy spectra. Thus, the statistical-mechanical equilibrium state contains a slight concentration of *surface intensified* energy near the radius of deformation.

d. Projection at the surface

It is not only the energetic transfers that differ in the case of nonuniform stratification, but their projection at the surface as well. In particular, in the case of oceanically realistic stratification, the surface signal reflects baroclinic modes more than it reflects barotropic modes when the two are comparable in magnitude, a result noted also by Wunsch (1997). Using an extensive collection of mooring data, he shows that variability in most of the extratropical ocean has its energy contained primarily in the barotropic and first baroclinic modes, but that *altimeter data* primarily reflects the first baroclinic mode, not the barotropic mode. If this is so, then we should *not* expect the satellite data to reflect the scale at which beta might affect or even arrest the inverse cascade, because the inverse cascade is largely a barotropic phenomenon.

In forced-dissipative flow, eddy generation by the

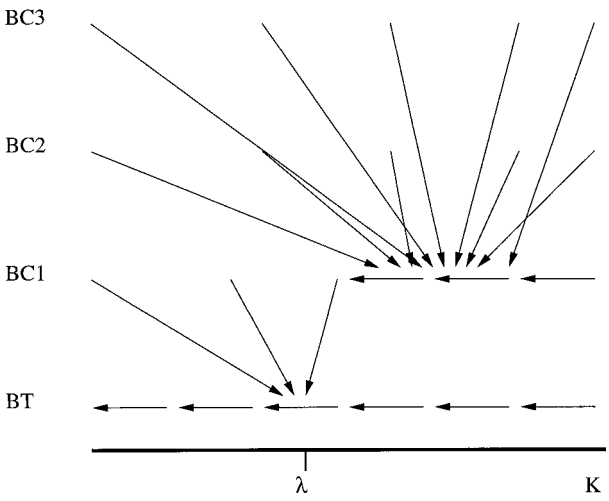

FIG. 4. Most likely energetic transfer paths as a function of vertical mode and horizontal scale (adapted from Fu and Flierl 1980).

TABLE 1. Summary of primary simulations considered. Here $N_{x,y}$ is horizontal resolution, N_z is vertical resolution, m_0 is initial mode, and K_0 is initial isotropic horizontal wavenumber. The first radius (λ_1) is a function of both δ_{tc} and the parameter F, which is the same for all runs and essentially determines the domain size. The term ''LIN'' as an entry for δ_{tc} implies that the stratification is uniform in this case (the density varies linearly with depth). Other parameters are as described in the appendix. The final column displays the final state baroclinicity ratio for each run.

Simulation	$N_{x,y}$	N_z	δ_{tc}	λ_1	β	m_0	K_0	ν	E_{bc}/E_{bt}
A	128	8	LIN	7.8	0	6	30	8×10^{-14}	1.1×10^{-2}
B	128	8	LIN	7.8	10	6	30	8×10^{-14}	1.7×10^{-3}
C	128	8	LIN	7.8	10	6	4	8×10^{-14}	4.4×10^{-3}
D	128	8	0.08	10.5	0	6	30	8×10^{-14}	1.1
E	128	8	0.08	10.5	10	6	30	8×10^{-14}	0.17
F	128	8	0.08	10.5	10	6	4	8×10^{-14}	0.22
G	128	8	0.08	10.5	10	1	4	8×10^{-14}	2.5×10^{-2}
H	256	8	LIN	14.6	25	6	5	8×10^{-16}	4.7×10^{-3}
I	256	8	0.05	23.7	25	6	5	8×10^{-16}	0.14
J	256	8	0.10	18.0	25	6	5	8×10^{-16}	0.15
K	256	8	0.20	14.2	25	6	5	8×10^{-16}	0.10
L	128	8	LIN	7.8	50	6	30	8×10^{-14}	2.7×10^{-3}
M	128	8	0.08	10.5	50	6	30	8×10^{-14}	0.11
N	128	8	0.20	8.2	0	6	30	8×10^{-14}	0.97
O	128	8	0.20	8.2	10	6	30	8×10^{-14}	0.15
P	128	8	0.20	8.2	50	6	30	8×10^{-14}	0.12

mean flow is independent of nonlinear internal transfers—that is, the eddy energy generation term in the energy budget is linear. For the surface intensified mean flows found in the ocean, eddy energy will be spawned predominantly in the baroclinic flow, so that if transfers to the barotropic mode are inhibited, while other transfers prefer to move energy to the first baroclinic mode, we might expect a residual concentration of energy in the first baroclinic mode *and* near the first deformation scale in steady-state flow as well. This, in combination with the expectation that baroclinic energy will be better represented in the surface signal than barotropic energy, may explain the finding that surface ocean eddy scales, calculated from TOPEX/Poseidon altimetry, are proportional to the local first radius of deformation (Stammer 1997).

5. Numerical simulations

Freely decaying simulations of geostrophic turbulence are performed to test some of the hypotheses set forth in section 4. The numerical model is described in the appendix, but is based on the horizontally spectral quasigeostrophic equation of 3.4. Primarily we are interested in two possible features. First, we would like to know whether the conjectures of Fu and Flierl (1980) are valid—that is, energy in high baroclinic modes should preferentially transfer to the first baroclinic mode before decaying to the barotropic mode. Second, according to arguments presented in section 4, transfers between high baroclinic modes should be *faster* than those to the barotropic mode. Additionally, we expect the equilibrium state to show a higher final ratio of baroclinic to barotropic energy, and expect the energy in the baroclinic mode to be peaked near the first baroclinic deformation wavenumber.

We initialize the simulations with energy contained solely in a given high baroclinic mode and at various horizontal isotropic wavenumbers, with initial total energy set to unity. The results are analyzed particularly in terms of two-dimensional spectra of kinetic energy as a function of vertical (modal) and isotropic horizontal wavenumber. Evolution is conveyed by a series of time slices taken at intervals of the eddy turnaround time, given by

$$\tau = \frac{2\pi}{\zeta_{\text{rms}}}, \tag{5.1}$$

where ζ_{rms} is the root-mean-square vorticity. (There is some subjectivity involved in choosing the proper rms vorticity, as it is not constant. The eddy turnaround timescale quickly settles down to a nearly constant value and we thus use an average that begins at the time when this value is close to its final value, and ends at the end of the simulation.) For all of the simulations considered here, we use eight vertical layers, and 128^2 or 256^2 equivalent horizontal gridpoints. The horizontal resolution is such that all of the baroclinic radii of deformation are resolved horizontally (Barnier et al. 1991 discusses the importance of this restriction).

The simulations presented are summarized in Table 1; refer to Fig. 5 for shapes of the density profiles.[1] Additionally, vertical mode structures corresponding to solutions of (3.6) for the uniform and most nonuniform profiles are shown in Fig. 6, in which the surface intensification of the modes for the thermoclinelike case is clear. The lower-resolution runs were performed pri-

[1] Note that the generating functional for the density profiles is given by (A.6), rather than a simple exponential. This expression is more a realistic representation of oceanic stratification, which still allows us to vary the thermocline depth/thickness with a single parameter.

marily as early tests, and we will concentrate primarily on the two runs with higher horizontal resolution, cases H and I. These cases also correspond to initialization at low wavenumber (large horizontal scales), which, for reasons discussed earlier and taken up again in the next section, is more representative of the scales at which eddy energy is generated by mean shear forcing in the ocean.

Time slices of the kinetic energy spectra for simulations H and I as functions of isotropic horizontal wavenumber, K, and vertical mode number, m, are shown in Figs. 7 and 8. It is clear that in the case with realistic stratification (simulation I), energy in high baroclinic modes decays preferentially to the first baroclinic mode, from where it cascades toward larger scale. Near the first radius of deformation (which is about 23 for case I), energy transfers to the barotropic mode and continues cascading to the largest scales. By contrast, in the case of simulation H (uniform stratification), energy cascades quite efficiently and directly to the barotropic mode (also near the first radius, which is about 15 for case H).

Figure 9 shows the baroclinicity, defined here as the ratio of all baroclinic energy to barotropic energy, versus eddy turnaround time for the four simulations A, B, D, and E. Runs A and B utilize uniform stratification, the *latter* includes the β effect while the former does not. Runs D and E use realistic stratification, and the difference between them is just as that between A and B. Each of these runs was initialized at high horizontal wavenumber ($K_0 = 30$) and high baroclinic mode ($m_0 = 6$). This set of simulations was chosen to demonstrate

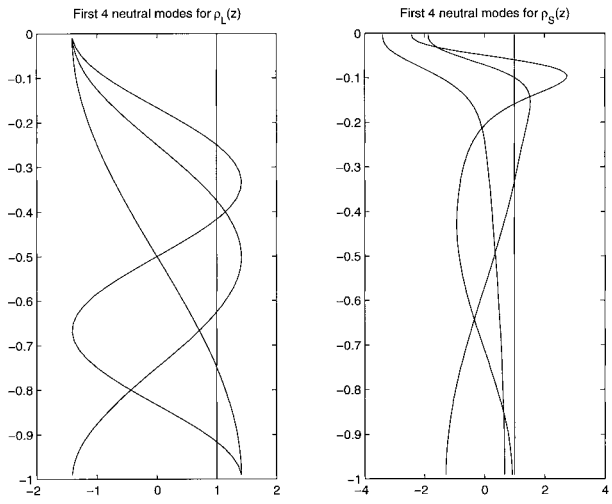

FIG. 6. Barotropic and first three baroclinic vertical modes for cases with uniform stratification (left) and with $\delta_{tc} = 0.05$ (right).

in the clearest possible fashion that the timescale on which conversion from baroclinic to barotropic energy occurs is a strong function of the stratification, as predicted. The magnitude and direction of the trend in the dependence of the baroclinicity on β is more surprising, and we have no strong argument to explain it—we take it as an interesting but empirical fact that β increases the efficiency of barotropization.

The wary reader may question whether the relative differences shown are a strong function of the particular numerical values chosen for the parameters. In fact,

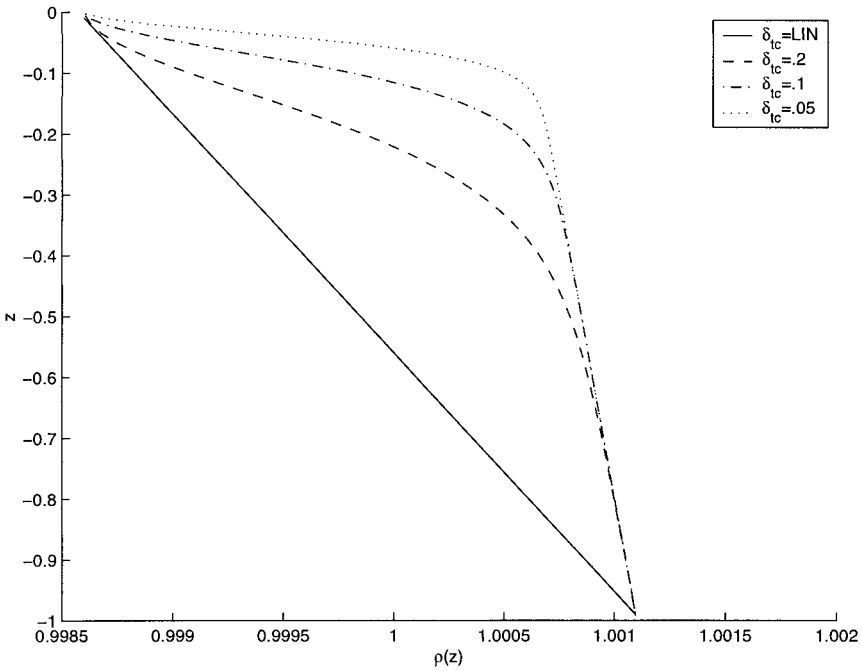

FIG. 5. Vertical profiles of density using (A.6) with $\Delta\rho = 0.002$ and $\alpha = 0.0005$.

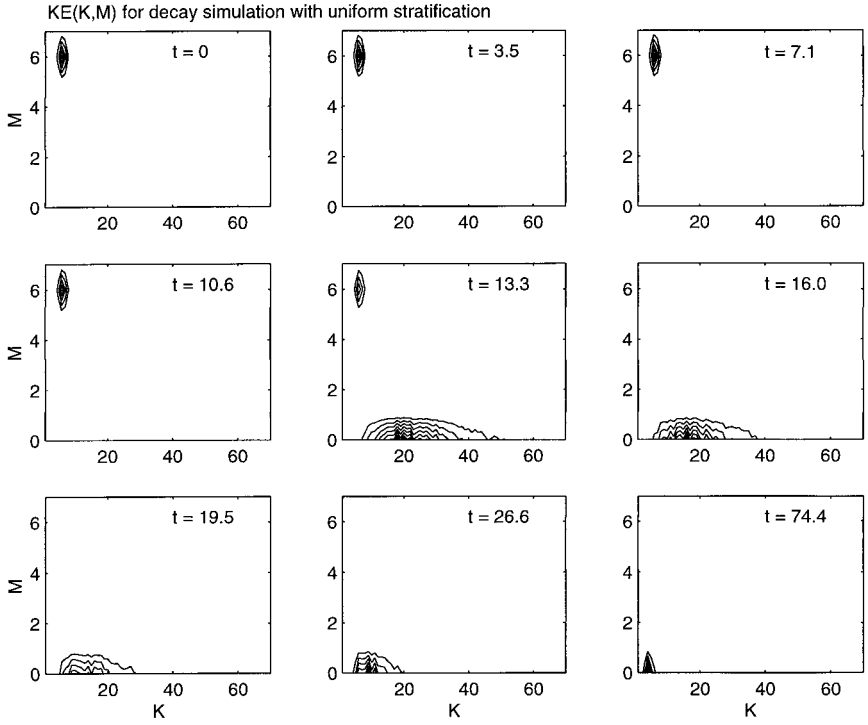

FIG. 7. Time sequence of kinetic energy spectra for decay simulation H. Times are given in terms of eddy turnaround time, τ_{eddy}, and axes are vertical mode number, M, and horizontal isotropic wavenumber, K. Contour values are linear over the range of values at each frame. The first radius of deformation is $\lambda_1 = 14.6$.

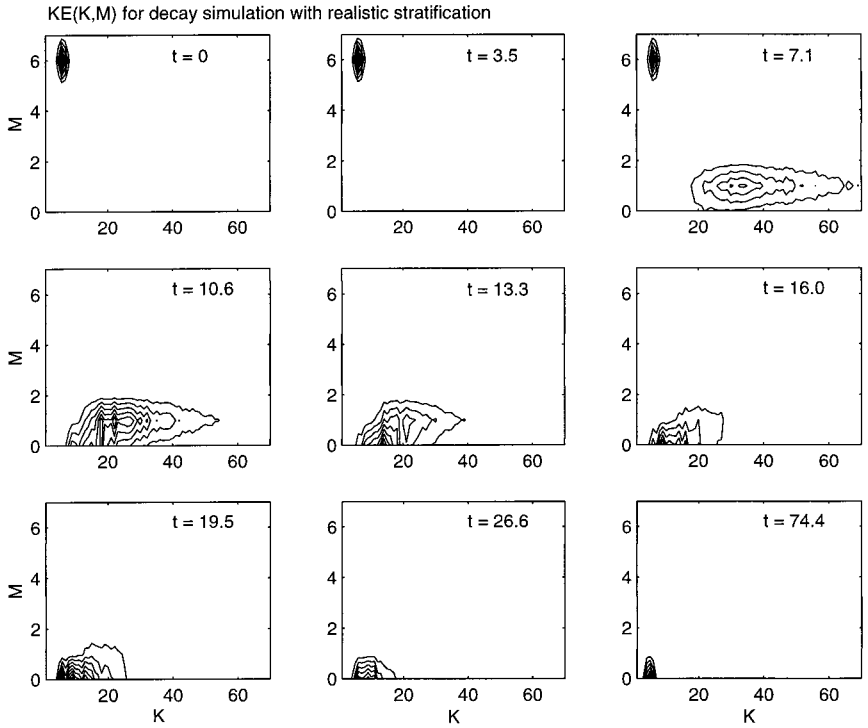

FIG. 8. As for Fig. 7, but for simulation I. In this case the first radius of deformation is $\lambda_1 = 23.7$.

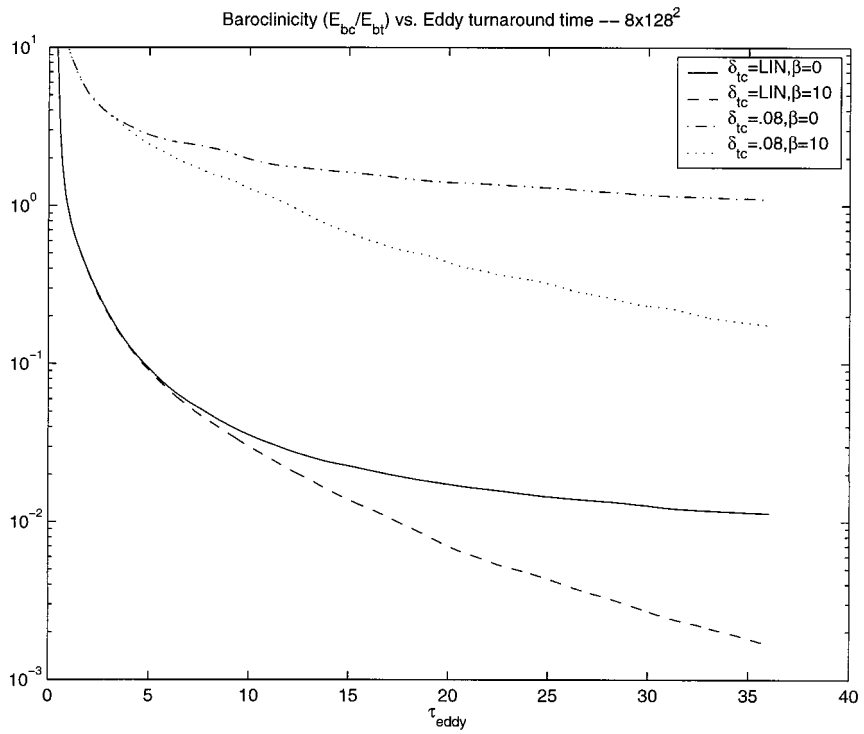

FIG. 9. Ratio of baroclinic to barotropic energies vs time (in units of eddy turnovers) for the decay simulations A, B, D, and E.

these four runs are part of a larger set of nine runs, the remainder including runs with each of the included stratification profiles, but with $\beta = 50$, and three runs with $\delta_{tc} = 0.2$ and $\beta = 0$, 10, 50 (these are runs L, M, N, O, and P in Table 1). The results of these runs are omitted to prevent clutter, as the differences are minor. In particular, the runs with weaker but still nonuniform stratification ($\delta = 0.2$) are barely different from the ones with strong stratification ($\delta = 0.08$). Moreover, increasing β to 50 in each case has a smaller effect (about 20%) than the initial jump from $\beta = 0$ to $\beta = 10$. The above results are also qualitatively similar to those initialized at low horizontal wavenumber, the primary difference being an initial timelag in the barotropization process due to the slow initial eddy turnaround times engendered by low wavenumber motion. Final state baroclinicities for all runs are tabulated in Table 1.

Given these facts, we can say with some generality that stratification profiles of the type found in the midoceans can increase the baroclinicity of eddying motion by nearly two orders of magnitude over that in the presence of uniform stratification. While one should keep in mind that these are spindown runs, and may differ *qualitatively* from forced-dissipative results, it is interesting to note that the final baroclinicity ratio for the realistic cases (D and E) are nearly unity, implying near equipartition between barotropic and first baroclinic energy, similar to the ratio determined by Wunsch (1997) for much of the midlatitude oceans. The results of studies such as Treguier and Hua (1988) imply that topography should increase this ratio even further, perhaps compensating for the decrease in baroclinicity due to β.

Now we will consider the spectral characteristics of central cases H and I, averages (over approximately the last five eddy turnaround times) of which are shown in Fig. 10. The top two panels show barotropic and first baroclinic kinetic, and available potential energies as functions of isotropic horizontal wavenumber. In the case with realistic stratification (right panels), note the positions of the peaks in the barotropic and baroclinic spectra—the barotropic spectra is peaked near $K = 5$, while the baroclinic spectrum is peaked near $K = 21$. The barotropic spectrum for the uniformly stratified case (left panels) is peaked in a similar position, but the baroclinic peak is at much higher K. Furthermore, there is utterly negligible energy remaining in the baroclinic mode.

With regard to the barotropic peaks, note that $\beta = 25$ in both cases. Since the energy of the problem varies by less than 50% from that at the beginning, the rms velocity does not change significantly, and we can thus calculate the Rhines scale. In terms of our choice of nondimensionalization, it turns out that $k_\beta = \sqrt{\beta}$, so that both of these cases have barotropic energy peaked near the predicted Rhines scale, $k_\beta = 5$.

The baroclinic peak for case I happens to lie very near the first radius of deformation for the stratification

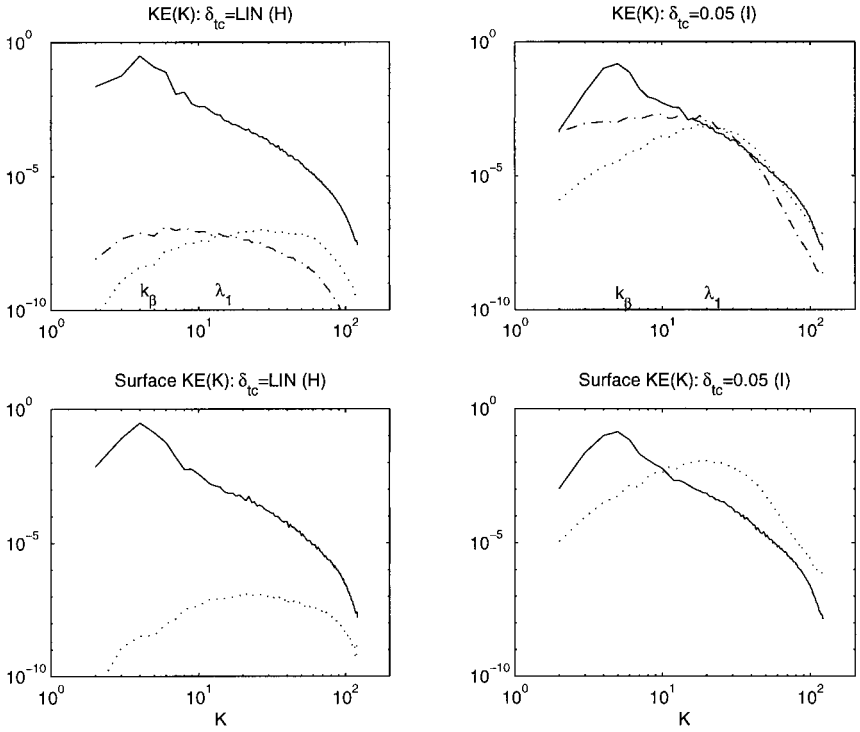

FIG. 10. Energy spectra for decay simulations H (on the left) and I (on the right). Top two plots show barotropic (solid), first baroclinic (dashed), and available potential energies. The bottom two figures show the barotropic (solid) and first baroclinic (dashed) kinetic energy spectra *at the surface* (the top model layer) for these two simulations. Averages were taken over the last five eddy turnaround times.

parameters used in this problem, while that of the uniformly stratified case does not, apparently. In order to quantify the possible relation between baroclinic kinetic energy peak position, we consider a scatterplot of peak maxima and first radii of deformation in Fig. 11. Apparently, for the realistically stratified cases, there is a relatively good correlation between these two quantities, as predicted.

Returning to Fig. 10, the bottom panels support yet another hypothesis made earlier. These panels represent the projections of the barotropic and first baroclinic modes onto the *surface* (or top model layer). In particular, if we set $z = 0$ in our vertical modal expansion (3.8), we have

$$\psi_{kl}(0) = \sum_{m=0}^{\infty} \Psi_{klm}\phi_m(0).$$

The bottom panels of the figure represent the first two terms of this expansion, as functions of isotropic wavenumber, $K = \sqrt{k^2 + l^2}$. The barotropic component does not change with this projection (since it is by definition independent of depth). The baroclinic component of case I (left), however, changes significantly—as expected from the findings of Wunsch (1997), the baroclinic mode is overrepresented at the surface. Nevertheless we should not overinterpret these results, for they represent decay simulations whose dynamics are fundamentally simpler than those of the forced-dissipative case, which are probably more representative of the situation in the ocean.

If it is indeed the β effect that is halting the cascade, then we expect anisotropy, at least in the barotropic mode (Rhines 1975; Vallis and Maltrud 1993). Figure 12 presents barotropic and baroclinic streamfunction snapshots from cases I and H to this effect. Both of the barotropic cases (left panels) show relatively strong zonal elongation. The anisotropy is less evident in the baroclinic fields, although at least in case I, there appears to be a slight degree of zonal elongation as well.

Finally, in Figs. 13 and 14 we show iso-vorticity plots of the two cases, H (top) and I (bottom). Each snapshot is of the last frame of the respective simulation. Isovorticity values are -9 and 9 for case H and -7 and 7 for case I—a higher value was required for the uniformly stratified case (H) in order to see any of the columnar vortex structures. Case I shows some columnar (barotropic) structures as well, but is dominated by the presence of coherent vortices, which are trapped above the thermocline. This situation stands in contrast to the simulations of, for example, McWilliams (1989), whose results are similar to our case H, showing a tendency toward depth-independent columnar vortices.

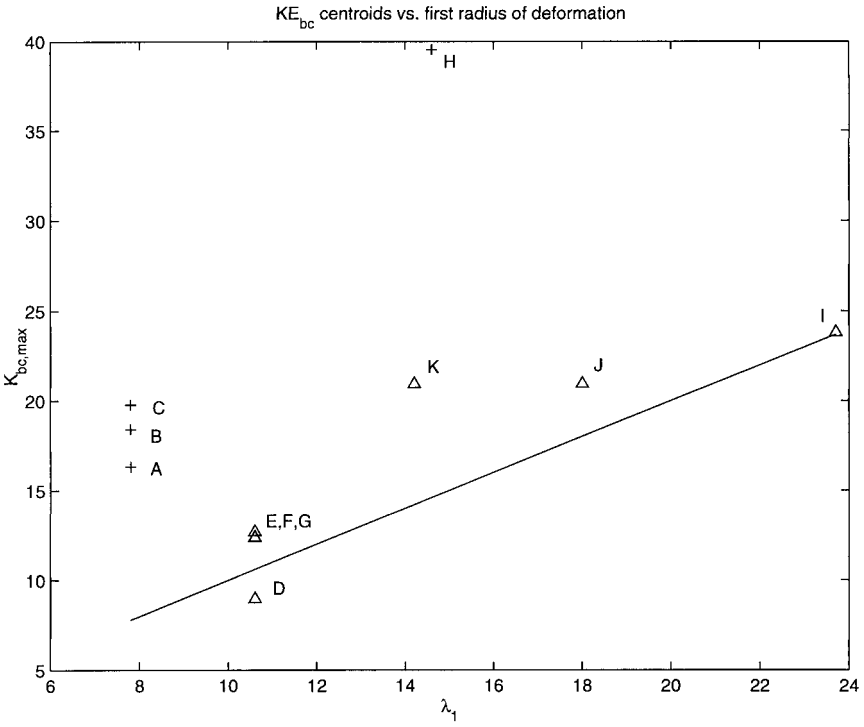

FIG. 11. Scatterplot of centroids of kinetic energy in sum of baroclinic modes for each simulation listed in Table 1 vs their respective first radius of deformation, λ. Realistically stratified cases are plotted with triangles, while those with uniform stratification are plotted with crosshairs.

There is a somewhat subtle issue that should be discussed here. The presence of relatively intense surface-trapped vortices occurs despite the fact that at the end of the simulation, most of the *energy* is barotropic. The energy comprising the surface-trapped vortices is certainly baroclinic and kinetic, so one might at first see a contradiction. In fact, though the bulk of the kinetic energy is barotropic, the vorticity *maxima* are apparently baroclinic, which is an allowable state of affairs in quasigeostrophic dynamics. A stability analysis for a vortex in the presence of nonuniform stratification might add clarity to this issue.

6. Conclusions

In a uniformly stratified background state, energy transfer in geostrophic turbulence is characterized by an inverse cascade toward the barotropic state—the system seeks the gravest state, both horizontally and vertically. In some contrast, if the stratification is nonuniform, and specifically if the stratification is characterized by an upper-ocean pycnocline, then both theoretical arguments and numerical simulation show that energy transfer to the barotropic mode is inhibited. Rather, energy in high baroclinic modes cascades preferentially toward the first baroclinic mode, and toward horizontal scales near the corresponding deformation scale of the first mode. Indeed numerical simulations show a correlation between the first radius of deformation and the peak in the final baroclinic kinetic energy spectrum. Baroclinic fields in the realistically stratified cases contain a strong population of near-surface coherent vortices, whereas the vortices in the uniformly stratified case have much greater vertical extent. And although the presence of a nonzero β effect will tend to aid in barotropization, the inhibiting effects of a nonuniform stratification are, in an oceanic parameter regime, overwhelmingly stronger.

Since the baroclinic mode projects substantially on the surface in the case of nonuniform, pynoclinelike stratification (see also Wunsch 1997), a concentration of eddy energy in the first baroclinic mode at the radius of deformation will be reflected in a corresponding concentration of variance in the surface height field, as observed by TOPEX/Poseidon. Nevertheless, the barotropic arrest scale, in the cases that included the β effect, is likely to be at or larger than the Rhines scale, k_β (at least in the flat- bottom case we have investigated). Numerical simulations indeed demonstrated this, with barotropic streamfunction contours becoming zonally elongated, while baroclinic fields exhibit only weak anisotropy. We thus conjecture that the barotropic scales of the ocean are both much larger and more anisotropic than the baroclinic scales. We also expect that mesoscale eddies may provide a nonnegligible source of abyssal motion. Current observational evidence is inconclusive on both of these points.

Our study has neglected a number of important pro-

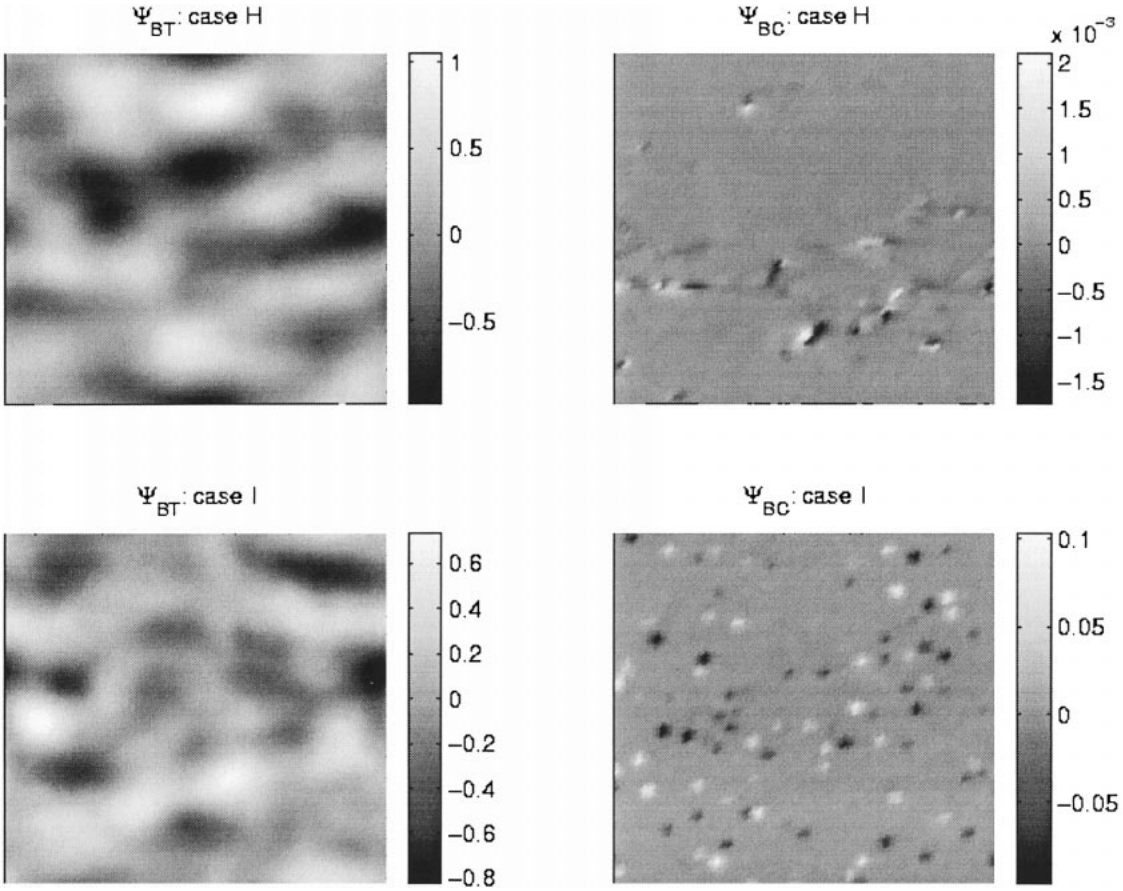

FIG. 12. Barotropic and baroclinic streamfunctions in the physical plane for cases H and I.

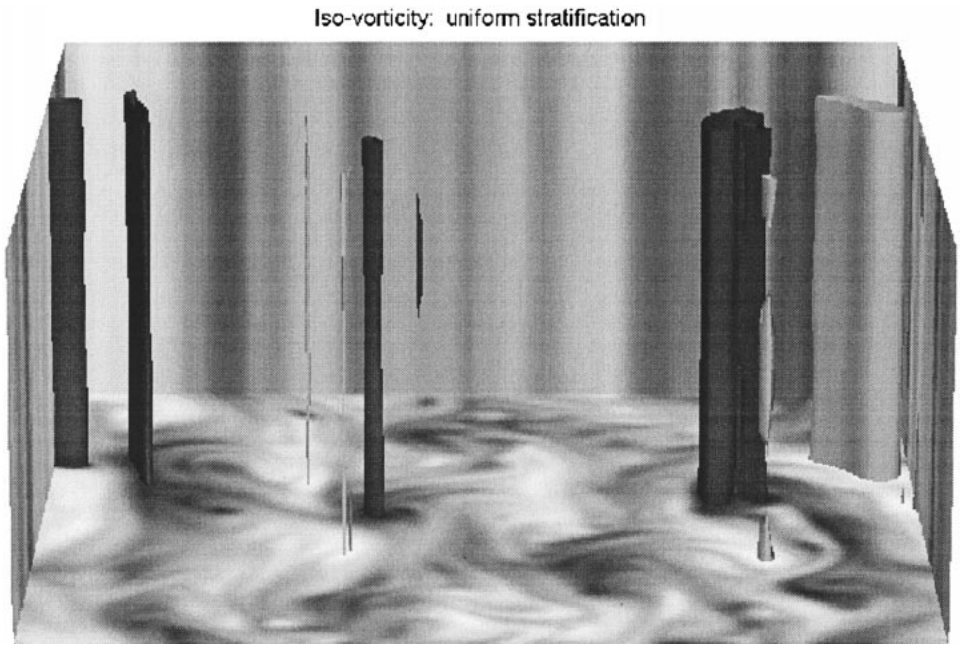

FIG. 13. Iso-vorticity plot of decay simulation H. Light and dark gray values are $\zeta = 7, -7$, respectively. Snapshot taken at $t \simeq 40\tau_{\text{eddy}}$.

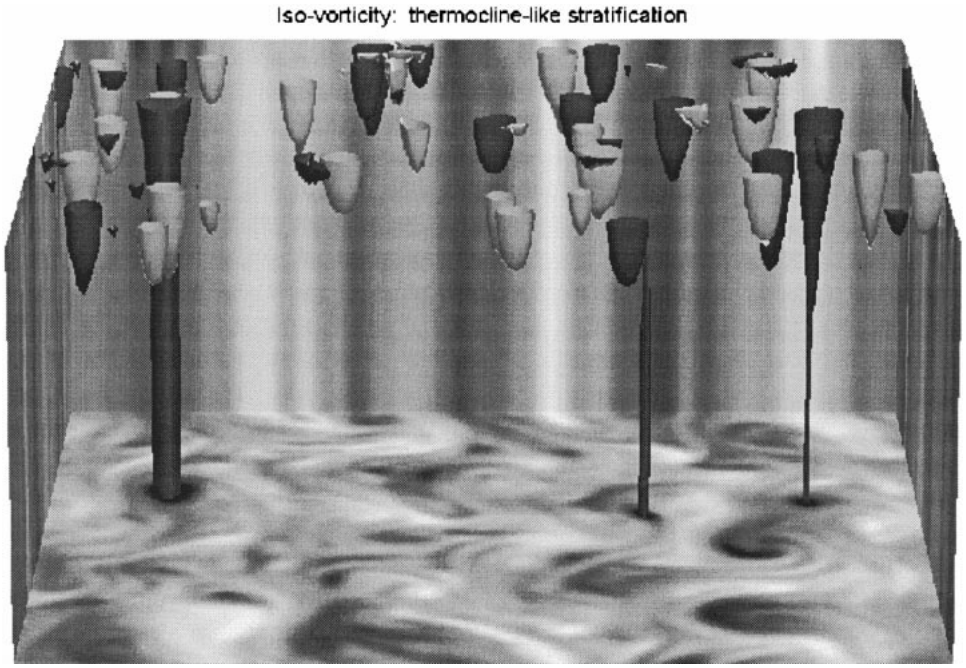

FIG. 14. Iso-vorticity plots of decay simulation I. Light and dark gray values are $\zeta = 9, -9$, respectively. Snapshot taken at $t \simeq 40\tau_{\text{eddy}}$.

cesses. In particular, the equilibration of oceanic eddies is ultimately a forced-dissipative process, with forcing arising from a baroclinically unstable background shear and the dissipation from lateral or bottom friction. These topics will be addressed in a forthcoming paper. Second, topographic effects are almost certainly important in increasing baroclinicity in the ocean (Treguier and Hua 1988), and possibly in scattering energy into small-scale, nongeostrophic motion thereby providing an indirect energy sink in addition to bottom drag. Inhomogeneity, lateral boundaries, and the presence of significant nonzonal mean flows (which are not stabilized by the β effect) are additional complicating factors.

Nevertheless, nonuniform stratification clearly has a first-order influence on the evolution of mesoscale eddies. It seems that the energetic pathways taken by geostrophic turbulence in the presence of such nonuniform stratification may be at least partly responsible for the concentration of energy at the first deformation scale, which would then, in turn, explain the observed surface scales of mesoscale eddies in the midlatitude oceans. Moreover, while the caveats of the previous paragraph will undoubtedly change some details of the picture, there is no reason to expect that the correlation between the deformation scale and the apparent scale of eddies (i.e., the dominance of the first baroclinic mode in the surface height field) will be altered by the inclusion of any such effects.

Acknowledgments. The authors wish to thank Bach-Lien Hua, Isaac Held, and Stephen Griffies for very helpful discussions regarding this work, which was largely funded by the ONR and the NSF.

APPENDIX

Numerical Model Details

The numerical model is based upon the layered, spectral quasigeostrophic equations, (3.4), which we nondimensionalize as follows (dimensional values are asterisked): $0 \le (x^*, y^*) \le L$ and $0 \le (x, y) \le 2\pi$, hence $(x^*, y^*) = \hat{L}(x, y)$, where $\hat{L} = L/2\pi$ (this scaling will yield integer wavenumbers for the horizontal spectral representation). Velocity is scaled as U (the vertical average of the mean zonal velocity profile), time is scaled as $\hat{L}/U$, and the following nondimensional parameters arise:

$$F = \frac{f_0^2 \hat{L}^2}{gH}, \qquad \beta = \frac{\beta_0 \hat{L}^2}{U}, \qquad \delta_n = \frac{H_n}{H},$$

in which H_n is the mean thickness of the nth layer, f_0 is the Coriolis frequency at some latitude θ_0, and $\beta_0 = (df/dy)_{\theta_0}$. The equation of motion (with all variables now nondimensional) is nearly the same as (3.4) with subscripts n added to denote the layer,

$$\dot{q}^{kln} + \hat{J}_{kl}(\psi_n, q_n) + ik(\overline{u}_n q_{kln} + \overline{q}_{n,y}\psi_{kln}) = -\nu K^8 q_{kln} + \kappa K^2 \psi_{kln}\delta_{n,N}, \tag{A.1}$$

for $n \in (1, N)$, where N is the bottom layer, and

$$q_{kln} = (-K^2 + F\Delta_n)\psi_{kln}. \quad \text{(A.2)}$$

In the above expression, Δ_n is the layer differencing operator, which replaces the vertical derivatives in (3.5), and is explicitly

$$\Delta_n\psi_n = \frac{1}{\delta_n}\left[\frac{1}{\rho_n - \rho_{n-1}}\psi_{n-1} - \left(\frac{1}{\rho_n - \rho_{n-1}} - \frac{1}{\rho_{n+1} - \rho_n}\right)\psi_n + \frac{1}{\rho_{n+1} - \rho_n}\psi_{n+1}\right], \quad \text{(A.3)}$$

in which $\rho_n = \rho_n^*/\rho_0$ is the nondimensional potential density of the nth layer. Here ρ_n is subsampled at layer centers.

Energetics for the layered representation follow as for the others—multiply (A.1) by $-\psi_{kln}^*$ and sum for total budgets. The kinetic and available potential energy spectra for layer n are, respectively,

$$\mathcal{K}_{kln} = K^2\rho_n\delta_n|\psi_{kln}|^2, \quad \text{(A.4)}$$

$$\mathcal{A}_{kln} = F\frac{|\psi_{kln+1} - \psi_{kln}|^2}{\rho_{n+1} - \rho_n}. \quad \text{(A.5)}$$

Budget and energy spectra are used to diagnose numerical results. In this usage, they are generally summed in shell-integral form over isotropic horizontal wavenumber, $K = \sqrt{k^2 + l^2}$.

The numerical model uses a leapfrog time step with a weak Robert filter, as well as an occasional Euler step in order to suppress the computational mode. Dissipation terms are time-lagged to avoid linear numerical instability. The nonlinear term is calculated via a dealiased spectral transform method (Orszag 1971) using isotropic truncation.

The potential density, $\rho(z)$ (where $z \in [0, -1]$ is now nondimensional) is set analytically via a function that mimics the basic shape observed in the ocean when internal parameters are set correctly. The function is

$$\rho(z) = [1 + \Delta\rho \tanh(z/\delta_{tc})^2](1 - az), \quad \text{(A.6)}$$

where $\Delta\rho$ is approximately the difference in the nondimensional densities at top and bottom, and the linear multiplicative function involving α approximates the roughly linear increase in density below the thermocline (which is the result of the small but nonnegligible dependence of seawater density on pressure). The parameter δ_{tc} is essentially the scale thickness, which sets the degree of surface intensification. Typical profiles in the midlatitude ocean have δ_{tc} between 0.05 and 0.15 and α between 10^{-4} and 10^{-3} (our simulations used $\alpha = 0.0005$).

The vertical discretization (i.e., the layer thicknesses, δ_n) is set by making the layer interfaces lie close to the zeros of the highest resolved vertical normal mode, following Beckman (1988). The discretization is obtained iteratively by calculating the normal modes first using a very large number of layers relative to the final number of layers (N) desired. The zeros of the resulting ($N - 1$)th eigenfunction are then used to set the operational discretization function, δ_n.

REFERENCES

Abromowitz, M., and I. A. Stegun, 1972: *Handbook of Mathematical Functions.* Dover, 1046 pp.

Barnier, B., B. L. Hua, and C. Le Provost, 1991: On the catalytic role of high baroclinic modes in eddy-driven large-scale circulations. *J. Phys. Oceanogr.,* **21,** 976–997.

Beckmann, A., 1988: Vertical structure of midlatitude mesoscale instabilities. *J. Phys. Oceanogr,* **18,** 1354–1371.

——, C. W. Böning, B. Brügge, and D. Stammer, 1994: On the generation and role of eddy variability in the central North Atlantic Ocean. *J. Geophys. Res.,* **99,** 20 381–20 391.

Charney, J. C., 1947: The dynamics of long waves in a baroclinic westerly current. *J. Meteor.,* **4,** 135–163.

———, 1971: Geostrophic turbulence. *J. Atomos. Sci.,* **28,** 1087–1095.

Chelton, D. B., R. A. deSzoeke, M. G. Schlax, K. El Naggar, and N. Siwertz, 1998: Geographic variability of the first baroclinic Rossby radius of deformation. *J. Phys. Oceanogr.,* **28,** 433–460.

Flierl, G. R., 1978: Models of vertical structure and the calibration of two-layer models. *Dyn. Atmos. Oceans,* **2,** 341–381.

Fu, L. L., and G. R. Flierl, 1980: Nonlinear energy and enstrophy transfers in a realistically stratified ocean. *Dyn. Atmos. Oceans,* **4,** 219–246.

Gill, A. E., J. S. A. Green, and A. J. Simmons, 1974: Energy partition in the large-scale ocean circulation and the production of mid-ocean eddies. *Deep-Sea Res.,* **21,** 499–528.

Hua, B. L., and D. B. Haidvogel, 1986: Numerical simulations of the vertical structure of quasi-geostrophic turbulence. *J. Atmos. Sci.,* **43,** 2923–2936.

Maltrud, M. E., and G. K. Vallis, 1991: Energy spectra and coherent structures in forced two-dimensional and beta-plane turbulence. *J. Fluid Mech.,* **228,** 321–342.

McWilliams, J. C., 1989: Statistical properties of decaying geostrophic turbulence. *J. Fluid Mech.,* **198,** 199–230.

Orszag, S. A., 1971: Numerical simulation of incompressible flows within simple boundaries: Accuracy. *J. Fluid Mech.,* **146,** 21–43.

Pedlosky, J., 1987: *Geophysical Fluid Dynamics.* Springer-Verlag, 710 pp.

Rhines, P. B., 1975: Waves and turbulence on a β-plane. *J. Fluid Mech.,* **69,** 417–443.

——, 1977: The dynamics of unsteady currents. *The Sea,* Vol. 6: *Marine Modeling,* E. D. Goldberg et al., Eds., Wiley and Sons, 129 pp.

——, and W. R. Young, 1982: Homogenization of potential vorticity in planetary gyres. *J. Fluid Mech.,* **122,** 347–367.

Salmon, R. S., 1980: Baroclinic instability and geostrophic turbulence. *Geophys. Astrophys. Fluid Dyn.,* **10,** 25–52.

——, G. Holloway, and M. C. Hendershott, 1976: The equilibrium statistical mechanics of simple quasi-geostrophic models. *J. Fluid Mech.,* **75,** 691–703.

Samelson, R. M., 1999: Note on a baroclinic analogue of vorticity defects in shear. *J. Fluid Mech.,* **382,** 367–373.

——, and G. K. Vallis, 1997: Large-scale flow with small diffusivity: The two thermocline limit. *J. Mar. Res.,* **55,** 223–275.

Stammer, D., 1997: Global characteristics of ocean variability estimated from regional TOPEX/Poseidon altimeter measurements. *J. Phys. Oceanogr.,* **27,** 1743–1769.

——, and C. W. Böning, 1992: Mesoscale variability in the Atlantic Ocean from Geosat altimetry and WOCE high-resolution numerical modeling. *J. Phys. Oceanogr.,* **22,** 732–752.

Stone, P., 1978: Baroclinic adjustment. *J. Atmos. Sci.,* **35,** 561–571.

Treguier, A. M., and B. L. Hua, 1988: Influence of bottom topography

on stratified quasi-geostrophic turbulence in the ocean. *Geophys. Astrophys. Fluid Dyn.,* **43,** 265–305.

Vallis, G. K., 1988: A numerical study of transport properties in eddy resolving and parameterized models. *Quart. J. Roy. Meteor. Soc.*, **114,** 183–204.

——, and M. E. Maltrud, 1993: Generation of mean flows and jets on a beta plane and over topography. *J. Phys. Oceanogr.*, **23,** 1346–1362.

Wunsch, C., 1997: The vertical partition of oceanic horizontal kinetic energy. *J. Phys. Oceanogr.*, **27,** 1770–1794.